Radio Science, Volume 33, Number 6, Pages 1641–1654, November–December 1998

Simultaneous meteor echo observations by large-aperture VHF and UHF radars

Q. H. Zhou and P. Perillat
Arecibo Observatory, National Astronomy and Ionosphere Center, Arecibo, Puerto Rico

J. Y. N. Cho
Department of Earth, Atmospheric, and Planetary Sciences, Massachusetts Institute of Technology, Cambridge

J. D. Mathews
Communications and Space Sciences Laboratory, Pennsylvania State University, State College

Abstract. We report simultaneous meteor echo observations using the Arecibo 430-MHz and 46.8-MHz radars. Using identical data-taking and meteor selection criteria, 1868 and 367 meteors were found in the 430-MHz and 46.8-MHz beams, respectively, while 145 were found in both beams during the 7 hours of observation. Of the 367 VHF echoes, there were only 10 trail echoes, while the rest were head echoes, which was quite contrary to expectation. The smaller number of meteors detected by the VHF system and its wider beam width show that UHF meteors are far smaller than the VHF meteors. We estimate that VHF head echoes have a typical effective scattering cross section of the order of 10^{-3} m^2, while the accompanying UHF echoes have an effective scattering cross section of the order of 10^{-6} m^2. The paucity of VHF trail echoes observed leads us to suggest that the ratio of head echo power to the trail echo power increases with decreasing meteor size. When a meteor is too small, a radar can observe the head echo but not the trail echo. Of the 145 meteors observed by both radars, the powers received by the two systems were not correlated. Although antenna beam pattern contributes to the lack of correlation, it is also possible that UHF and VHF echoes may be enhanced by different scattering mechanisms.

1. Introduction

Recent meteor observations using the world's most powerful UHF and VHF radars reveal unexpected echo characteristics. Using the Jicamarca 49-MHz radar, *Chapin and Kudeki* [1994a, b] reported that a large number of meteor echoes last over 15 s and attributed the characteristic to be due to plasma instability associated with equatorial electrojets. *Wannberg et al.* [1996] reported simultaneous observations using the European incoherent scatter (EISCAT) VHF and UHF radars. These authors found that their observations can be best explained by Rayleigh scattering from an overdense plasma coma. The observations by the Arecibo 430-MHz radar suggest that echo strength peaks in the head-on direction [*Zhou and Kelley*, 1997], which cannot be readily explained by existing theories. Other recent UHF observations include those by *Pellinen-Wannberg and Wannberg* [1994], *Zhou et al.* [1995], and *Mathews et al.* [1997].

In this paper, we report simultaneous meteor observations using the Arecibo 430-MHz and 46.8-MHz systems and discuss their implications. Previous multiple wavelength meteor studies include those by *Baggaley and Fisher* [1980], *Steel and Elford,* [1991] and *Wannberg et al.* [1996]. *Baggaley and Fisher* [1980] used three VHF frequencies (26, 69, 148 MHz) to study the initial radius effect of meteor trails. *Steel and Elford* [1991] compared the height distributions of meteors detected at different frequencies (2, 6, 26, and

Paper number 98RS02430.
0048-6604/98/98RS-02430$11.00

54 MHz). *Wannberg et al.* [1996] studied the head echoes using two higher frequencies (224 and 931 MHz). The two frequencies used in our current study are widely separated. The frequency of our VHF radar, 46.8 MHz, is similar to that of a meteor wind radar, which makes use of long-duration meteor trails to measure neutral winds. Our UHF radar, on the other hand, sees primarily head echoes [*Mathews et al.*, 1997; *Zhou and Kelley*, 1997]. The current simultaneous observation at 46.8 MHz and 430 MHz was hoped to offer some clues to the relation between head echoes and trail echoes. The results, however, show that like our UHF observations, the VHF echo characteristics cannot be extrapolated from observations using smaller radars. Some of the unusual characteristics are apparently due to the large antenna aperture used, which makes the radar very sensitive to faint meteors within a very small beam width. We briefly describe the radar systems and the data analysis procedure in section 2. Observational results are presented in section 3. Our emphasis will be on the VHF results since this is the first time that an aperture as large as 250 m in diameter has been used for VHF meteor observations. In section 4, we discuss some potential implications of the observation, and the major results are summarized in section 5.

2. System Parameters and Data Analysis

The two antennae that we used are the Arecibo UHF (430-MHz) and VHF (46.8-MHz) systems. The VHF radar is a "four-Yagi" point feed mounted concentrically with the UHF line feed. The two feeds share the same 305-m-in-diameter dish, with the UHF feed illuminating almost the full dish and the VHF feed illuminating 70% of the full dish. The system and relevant experiment parameters are listed in Table 1. During the observation, the two radars were synchronized by the same radar controller so that the interpulse period (IPP), pulse width, and sampling gate width were identical.

The observation was conducted on the night of September 29-30, 1994. In order to have a wider altitude coverage and a sufficient height resolution, we used a 5-ms IPP so that the tape drive could keep up with the data rate. Since the range resolution was 300 m, fast meteors without any trail may appear only once at each range gate. Such a setup dictates that we do not have the luxury of using multiple consecutive echoes in the same range gate for meteor detection like we did in our previous 430-MHz study [*Zhou and Kelley*, 1997]. With one point at one range gate detection, we found a total of 4337 meteor candidates in the 430-MHz radar and 2144 in the 46.8-MHz radar. To ensure the cleanness of the data, we required a candidate meteor to be detected at two consecutive range gates at nearly the same time. With two consecutive range gate detection, the total numbers of detections are reduced to 1868 and 367 for the 430-MHz and 46.8-MHz systems, respectively. In this paper, we will only consider the detections at two consecutive range gates as meteors. During the 7 hours of observation, 145 meteors were detected by both systems.

It should be noted that the 5-ms IPP may not be able to detect some cross-beam meteors. Our UHF system has an effective beam diameter of 300 m at 100 km. This means that the fastest cross-beam meteors may not be detected since only 4 ms are needed for meteors having a velocity of 70 km s^{-1} to cross the half-power beam width. However, because of the generally strong power of a meteor echo, a meteor can still be detected beyond the half-power beam width, especially considering that at 100 km, the UHF radar

Table 1. System Parameters

	VHF	UHF
Frequency, MHz	46.8	430
Three-decibel beam radius, deg	0.95 (1.65 km at 100 km)	0.085 (150 m at 100 km)
Main lobe gain	~41 dB	~60 dB at 100 km
Nominal peak transmitter power	~35 KW	2.5 MW
Noise temperature, K	~6000	70
IF filter	1-MHz Butterworth	1-MHz Butterworth
Interpulse period, ms	5	5
RF pulse width, μs	2	2
Receiving gate width, μs	2	2
Altitude coverage, km	69-118	69-118
Zenith, deg	8.8	8.8
Azimuth, deg	327 (0=N, 90=E)	327 (0=N, 90=E)

is well within the near-field range. (Far-field distance for the 430-MHz radar begins at about 260 km.) Another factor that affects the detection of cross-beam meteors is our requirement for a meteor to appear at two consecutive range gates. The returned power for a point target normally spreads over two range gates as a result of nonzero transmitter pulse length and finite filter bandwidth, although it is possible that the power at one of the two range gates may be below the threshold. Since this applies only to meteors strictly traveling perpendicular to the radar beam, it must be very rare. For a slightly oblique meteor, it is likely that a VHF meteor will physically cross over two range gates or more within the beam, thus lowering the number of meteors missed by the detection method.

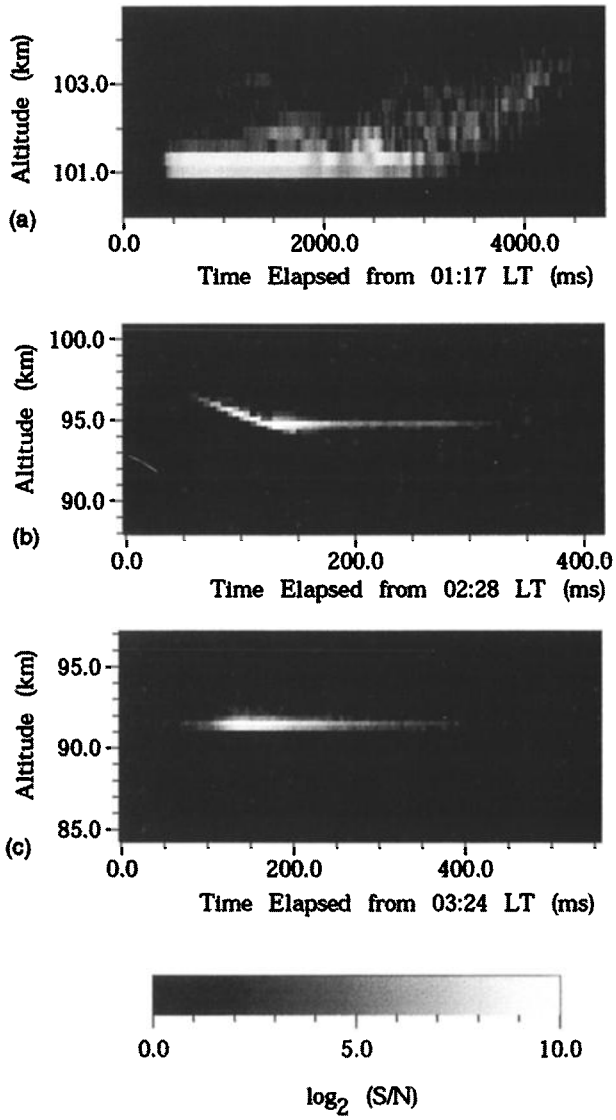

Figure 1. Three type 1 meteor echoes observed by the VHF radar. This type of echo was confined mainly within two range gates over an extended period (>200 ms).

3. Observations

The VHF echoes in our observation can be organized into three different types according to their range versus time characteristics, as illustrated in Figures 1 and 2 and Plate 1. Type 1 echoes, as shown in Figure 1, are distinguished by an extended detection period (>200 ms) in only one or two range gates. Such echoes may or may not be accompanied by a head echo such as the one presented in Figure 1b. Type 2 echoes exhibit a clear head echo followed by a long-duration echo that extends over more than three range gates. Of the three type 2 echo examples presented in Plate 1, two of them exhibit a temporal gap between the head echo and the trail echo. The third type is illustrated in Figure 2a and is characteristic of a head echo. During the 7 hours of observation, the number for the type 1, 2, and 3 echoes observed by the VHF

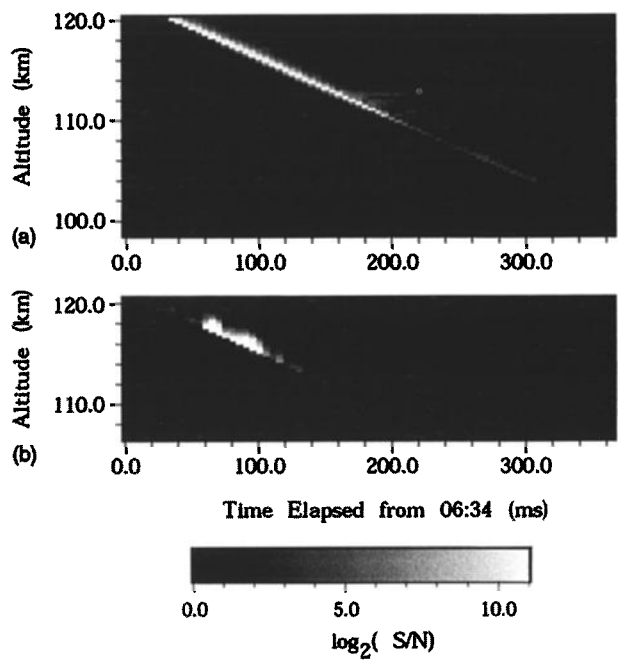

Figure 2. A head echo simultaneously observed by (a) the VHF radar and (b) the UHF radar. The meteor velocity is about 66 km s^{-1}. A VHF head echo is also designated as a type 3 echo in the text.

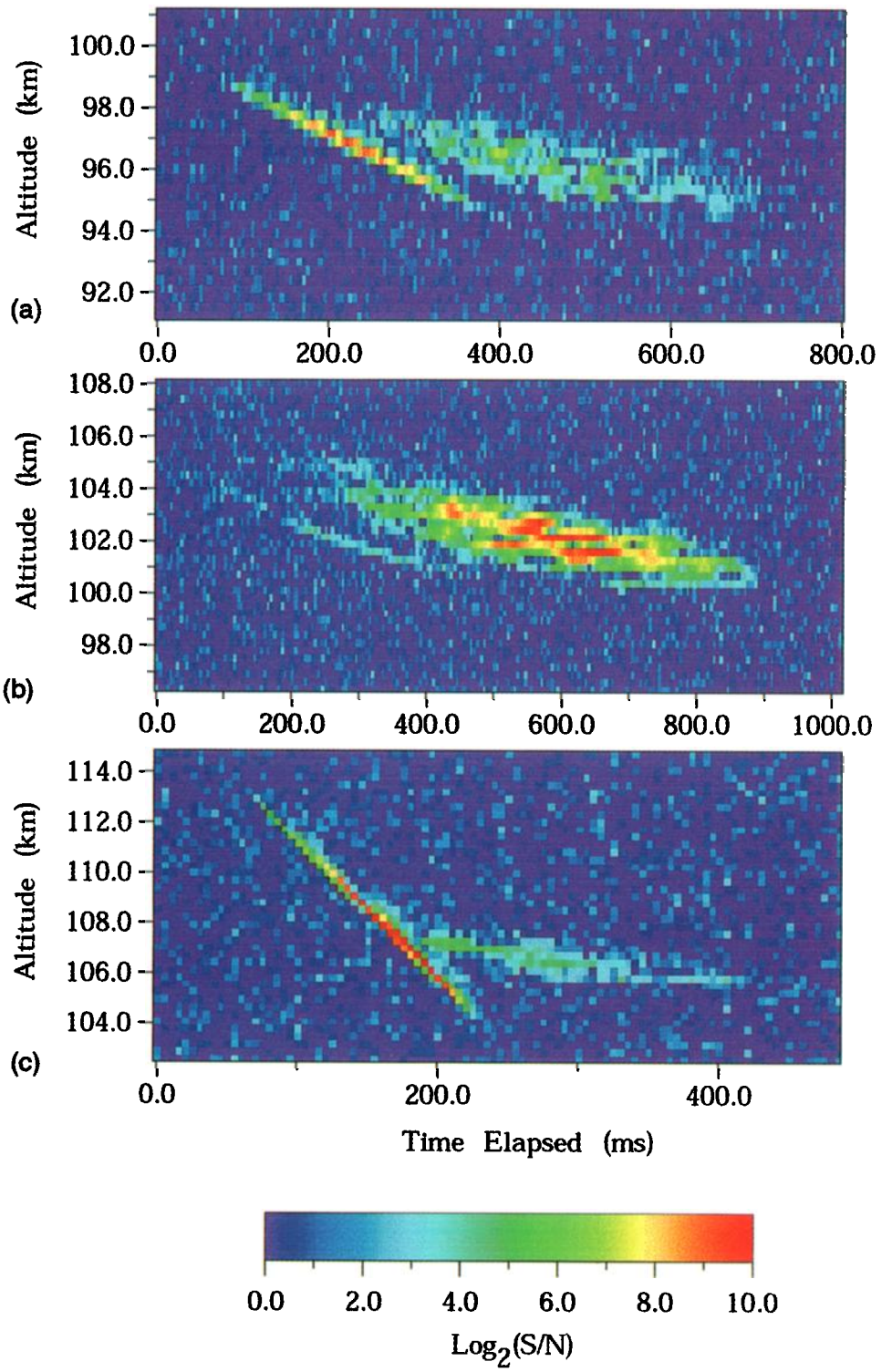

Plate 1. Three type 2 meteor echoes observed by the VHF radar. This type of echo has a visible head echo and a trail echo extending over more than three range gates. The line-of-sight velocities of the head echoes are (a) 14 km s^{-1}, (b) 9 km s^{-1}, and (c) 54 km s^{-1}. The corresponding local times were 0337, 0439, and 0531, respectively.

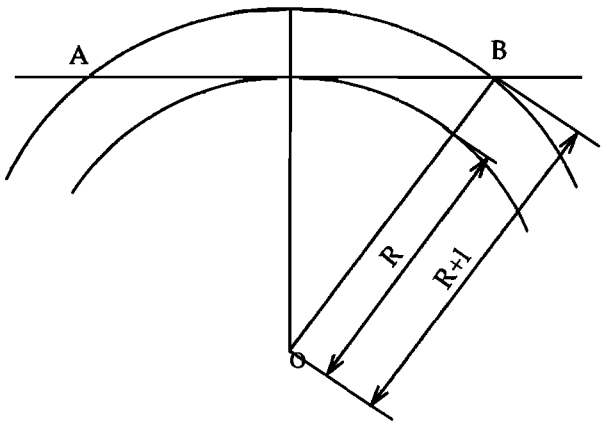

Figure 3. Depiction of a meteor traversing the radar beam. The two concentric arcs are separated by the range resolution l. AB is tangent to the inner arc. The maximum distance for the meteor to remain within one range gate is AB, which equals $2(2Rl)^{1/2}$.

radar was 7, 3, and 357, respectively. The UHF echoes were primarily head echoes, as typified by Figure 2b. In the following, we discuss these characteristic echoes in some detail.

3.1. Type 1 Echoes

Since there is an extended time period with essentially no temporal change in the echoing range, it is possible that some of the type 1 meteors were observed in the classical viewing geometry, that is, in which the radar beam is perpendicular to the meteor trajectory. One example is the echo shown in Figure 1c. In this viewing geometry, a head echo cannot be easily distinguished from a trail echo by just looking at the range-time plot. In the following, we estimate the meteoroid flight time within one range gate.

When a meteoroid travels perpendicular to the radar line of sight, the time it can stay within one range gate, with a range resolution l, is determined by

$$t = \frac{\min(\text{beam width}, 2\sqrt{2Rl})}{V} \quad (1)$$

where R is the shortest distance between the meteor trajectory and the radar, V is the meteor velocity, and min is the minimum operator. The second term in the parentheses is illustrated in Figure 3. The half-power beam width is approximately 3 km, and the second term in the parentheses is about 15 km assuming R=100 km and l=300 m. Therefore, if the meteor is detected only within the main lobe of the antenna, the meteoroid flight time within each range gate is predominantly determined by the beam width and is approximately 3 km/V. However, it is possible that echoes may be detected in the sidelobes, which would effectively increase the beam width. In such cases, the meteoroid flight time within each gate is at most 15 km/V. Since the minimum meteor velocity is 11.2 km s^{-1} without considering deceleration due to atmospheric resistance (which is seen not to be important for the meteors in our observation), the maximum time that a meteor can stay within a range gate of 300 m is approximately 1.4 s. This suggests that any type 1 echo having a duration longer than 1.4 s necessarily contains a trail portion. This is the case in Figure 1a. Since the other type 1 echoes lasted less than 1.4 s, the total time duration is of little help in identifying whether they are head echoes or trail echoes. To help identify whether an echo is a head or trail echo, we plot, in Figure 4, the received power at the height where the echo lasted the longest for six of the seven type 1 echoes. The seventh type 1 echo was observed at 0604 LT and was similar to the one shown in Figure 4f except that it was much weaker and will receive no further attention.

The echoes in Figure 4b-4f exhibit a well-defined signal strength decay constant before they became invisible. The smooth decay is indicative of a classical underdense echo. The decrease in echo strength for the underdense echo is due to the increase in trail diameter resulting from ambipolar diffusion. The decaying process is well understood, and the theoretical e-folding constant τ_t is related to the diffusion constant D through

$$\tau_t = \lambda^2/(32\pi^2 D) \quad (2)$$

where λ is the radar wavelength [e.g., *Djuth and Elder*, 1993]. Subject to some uncertainties, D can be considered known. For the purpose of comparison, we will use the ambipolar diffusion coefficient derived by *Greenhow and Neufeld* [1955],

$$\log_{10} D = 0.067H - 5.6 \quad (3)$$

where H is altitude, in kilometers. Using equations (2) and (3), we can compare the reference e-folding constant with that of the measured one to infer whether an echo belongs to the classical underdense type or not.

In Table 2, we list various measured parameters along with some theoretical calculations. The echoes are tabulated in descending altitude. The "figure" col-

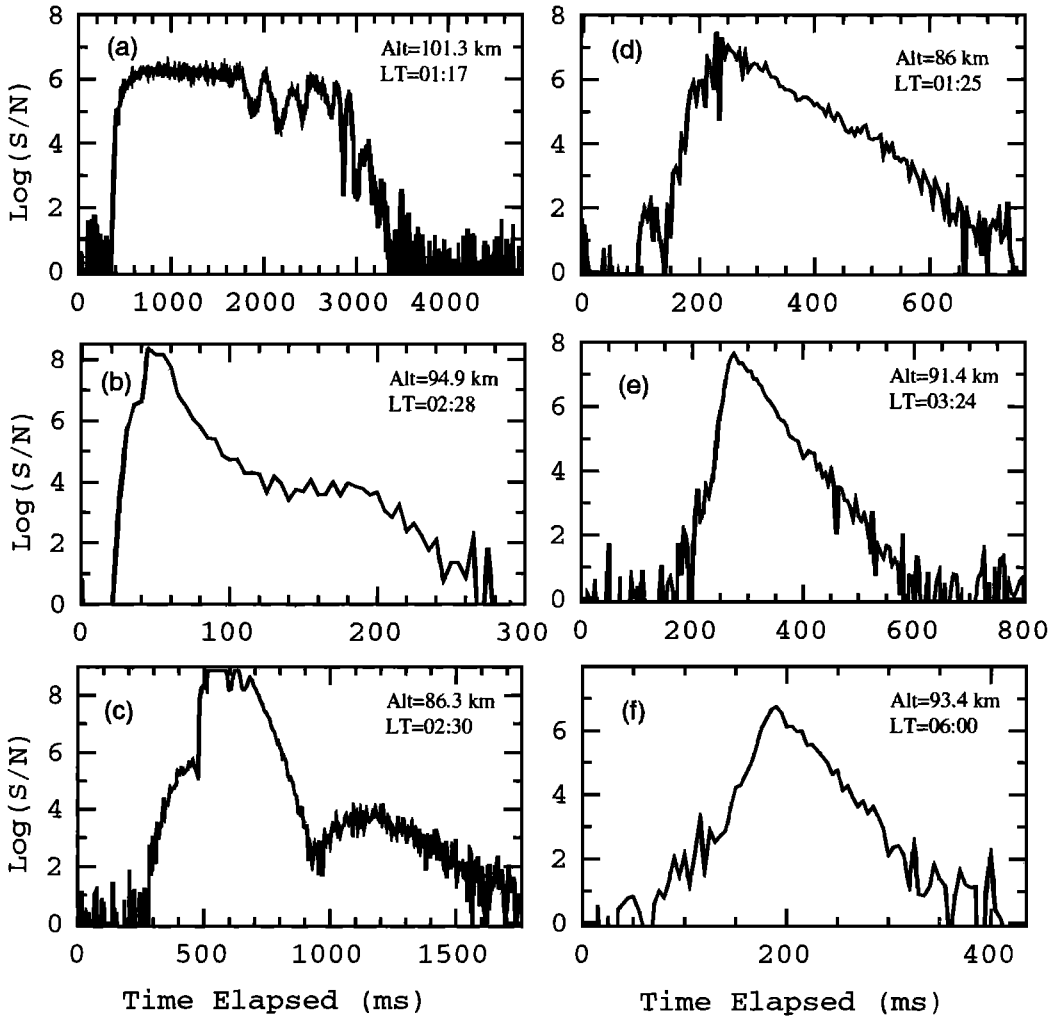

Figure 4. Echo power (in natural logarithm) as a function of time for six type 1 echoes.

umn indicates the figure number where the corresponding echo is shown. Here τ_m is the measured *e*-folding constant (i.e., the inverse of the slopes in Figure 4), τ_t is the theoretical *e*-folding constant as derived from equation (2), and τ_{ov} is the overdense time constant, which is discussed along with q/q_{tr} in the next paragraph. For the two echoes shown in Figures 4b and 4c, the listed value of τ_m is measured from the last slope. The theoretical value τ_t and the measured value τ_m are in good agreement except for the echo at 86.3 km. It is possible that this echo was detected far from the main lobe of the antenna. The discrepancy could be explained by assuming that the echo was detected about 15° off the beam center, which would lower the altitude by ~3.5 km. *Nakamura et al.* [1991] showed that the majority of the echoes observed by the middle and upper atmosphere (MU) radar were more than 15° off the beam center. It is possible that some of the echoes in our observation may actually be far away from the beam center, although we do not expect the majority of our echoes to be as far off the beam center as the echoes observed by Nakamura et al. This is because the off-center gain of our antenna drops much faster than the MU radar. Clearly, one needs a large number of samples to truly determine the decay time at each altitude and assess the sidelobe effect. Nevertheless, underdense diffusion appears to be the most plausible explanation for the decays exhibited in Figures 4d-4f and also possibly for the echoes shown in Figures 4b and 4c.

It is evident from Figure 4 that not all the type 1 echoes are the same. The echoes shown in Figures 4d

Table 2. Type I Echo Characteristics

Altitude, km	Time, LT	Figure	τ_m, ms	τ_t, ms	D, m^2/s	τ_{ov}, ms	q/q_{tr}
101.3	0117	1a, 4a	NA	9	15	1500	NA (70)
94.9	0228	1b, 4b	26	22	5.73	100	2.0 (1.7)
93.4	0600	4f	30	28	4.55		
91.4	0324	1c, 4e	44	39	3.34		
86.3	0230	4c	170	85	1.52	200	1.84 (0.92)
86.0	0125	4d	88	89	1.45		

NA, not available.

to 4f show a gradual increase in power and then a consistent decay. These three echoes are similar to the ones shown by *Djuth and Elder* [1993] from which neutral winds can be determined. The echoes shown in Figures 4a to 4c are more complicated and cannot be explained by classical underdense scattering alone. It is possible that overdense scattering and/or head echo scattering are also involved. When the trail is overdense, the power received does not change very much as long as the trail remains overdense [*McKinley*, 1961, p. 217]. For an overdense meteor, the electron line density is related to the duration time τ_{ov} via the following equation:

$$\tau_{ov} = \frac{\lambda^2 q}{4\pi^3 D q_{tr}} \tag{4}$$

where q is the electron line density and q_{tr} is the transition electron line density at which a meteor trail turns from overdense to underdense [*McKinley*, 1961]. From the above equation, we can use the duration time to calculate q/q_{tr} to see if it is larger than one, which is a necessary condition for a trail to be overdense. In Table 2, τ_{ov} is the duration time at which the power is approximately constant, and we assume this is the overdense duration time. For the echo shown in Figure 4b, we assume the overdense period is from 100 ms to 200 ms. In Figure 4c, the echo was saturated for the flat portion between 500 and 600 ms. It is possible that the actual echo power may not be the same during this period. If this is indeed the case, this echo may not be overdense. The q/q_{tr} values without parentheses in Table 2 are based on the measured ambipolar diffusion coefficients, while the values within the parentheses are based on the theoretical ambipolar diffusion. The q/q_{tr} values suggest that the echoes in Figures 4a and 4b are likely overdense echoes, while the echo in Figure 4c is at the border line of being overdense. In theory, the power of an overdense echo is proportional to the square root of the duration time if the antenna gain remains the same [*McKinley*, 1961]. In practice, however, since echoes are observed with different antenna gain due to their different locations in the sky, the power observed may not bear any relation to overdense duration time for a very small sample of echoes. The lower power and the longer duration of the echo shown in Figure 4a may indicate that this echo is observed farther off the beam center than the echo shown in Figure 4b.

For the echo shown in Figure 4b, a head echo was also observed, as seen from Figure 1b. The head echo shows a line-of-sight velocity of 30 km s^{-1}. This suggests that the meteor trajectory was off-specular by at least 25° by assuming a maximum heliocentric velocity of 70 km s^{-1}. The underdense scattering power for this echo thus cannot come from the classical specular effect of a transverse viewing geometry but more likely comes from an irregular deposition of ionization. As seen from Figure 1b, the head echo had an explosive ending, which is suggestive of intensive ionization at the end of the life of this meteoroid. As seen from Figure 4b, it appears that the "chronology" of this echo can be largely divided into three stages: (1) head echo, which lasts from 30 to 80 ms; (2) overdense scattering, which lasts from 80 to 200 ms; and (3) underdense scattering, which lasts from 200 to 260 ms. The echo shown in Figure 4c perhaps can be similarly classified.

One concern that we had was whether any of the echoes shown in Figure 4 could be due to satellite or orbital debris. Although in theory a satellite or space debris can be aliased into the meteor zone, satellite or space debris have the following two characteristics: (1) Their duration time is longer due to wider beam radius at higher altitude and slow orbital velocity (less than 11 km s^{-1}). For example, at 500 km altitude and 10 km s^{-1} tangential velocity, it takes more than 1.6 s to traverse the main lobe. (2) Satellite echoes are more or less symmetric with respect to maximum power. Obviously, none of the echoes shown in Figure 4 have

the above two characteristics simultaneously. Therefore we believe that all the echoes shown in Figure 4 are genuine meteor echoes.

3.2. Type 2 VHF Echoes

We now turn our attention to the second type of echoes observed. These echoes are rather similar to the extreme case echoes given by *McKinley* [1961, p. 224], except the echoes in our observation have a much shorter timescale. The delay between the head echo and the trail echo has been previously explained to be due to either the distortion of the trail by wind shear (glint theory) or uneven ionization (blob theory) [*McKinley*, 1961]. In the glint model the delay is due to the finite time needed to establish one or more specular reflecting zones as the trails become distorted by gravity waves. In the blob model, small discrete overdense "blobs" are assumed to be deposited as the meteor plunges into the atmosphere. The delay between the head and the trail echo is due to the time needed for the blobs to expand large enough to be detected by the radar while remaining overdense. To explain the large range extension of the trail echoes, we agree with the basic postulate of both the glint and the blob theories that the scattering medium needs to be overdense since underdense scatterings from different Fresnel zones are likely to render the power negligible. However, since the delay time between the head echo and the trail echo in our observation is less than 100 ms, the applicability of the glint or the blob theory to our observation may not be taken for granted. For example, the first echo shown in Plate 1a has a line-of-sight velocity of 14 km s^{-1}. This suggests that the meteor trail is off specular by at least 10^{o}, again by assuming a maximum meteor velocity of 70 km s^{-1}. For such a geometry, the delay time between the head echo and the trail echo predicted by the glint theory is at least 2 s [*McKinley*, 1961, p. 221]. It is possible that the blob theory together with the fragmentation hypothesis may be more applicable to our observation, which we further discuss next.

Simple blob theory appears to imply that the echo power as a function of time should be more or less smooth. This, however, is not the case for the type 2 echoes in our observation. This can be better seen from Figure 5, which shows the power variation as a

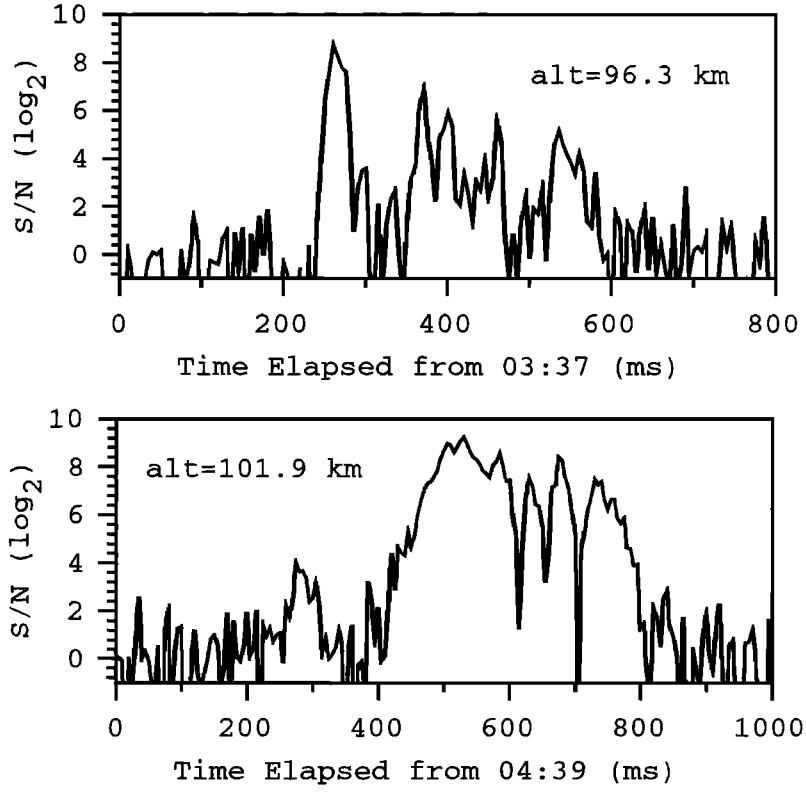

Figure 5. Echo power as a function of time for (a) the echo shown in Plate 1a at 96.3 km and (b) the echo shown in Plate 1b at 101.9 km.

function of time at a selected altitude from Plates 1a and 1b. The echo at 300 ms in both Figures 5a and 5b is the head echo. The trail echo begins at about 350 ms in both figures. The signal-to-noise ratio (SNR) changes from 1 to about 100 in 15 ms for both cases. The large temporal fluctuation of the echo power may imply the existence of multiple overdense blobs arriving at different times. Fragmentation, which is known to occur very frequently for large meteors at least [*Meisel et al.*, 1995], can provide multiple scattering centers. The broken-up pieces of a meteoroid may fly in different directions after their separation from the parent body or have different decelerations to create different arrival times at a certain range. In the extreme case of fragmentation, the scattering medium may be composed of charged dust, as observed by *Kelley et al.* [1998].

In addition, we note that the ratio of the head echo power to the trail echo power in type 2 echoes appears to increase with the line-of-sight velocity, as seen from Plate 1. However, since there are only three such echoes observed, this could just be fortuitous. Of all the 10 VHF type 1 and type 2 echoes, only one was accompanied by a weak UHF head echo. Although we believe that both type 1 and type 2 echoes are from relatively large meteors, it is likely that they were observed in the sidelobes of the UHF beam (and perhaps in the sidelobes of the VHF beam as well).

3.3. Type 3 VHF Echoes and UHF (Head) Echoes

As we mentioned earlier, head echoes were the most abundant in our observation. An example of a head echo simultaneously observed by both the VHF and UHF systems is shown in Figure 2. The VHF head echoes, in general, have a very large radial velocity, suggesting that their trajectories are usually not perpendicular to the radar line-of-sight direction. The much longer VHF echo extension can at least partially be due to the much larger beam width of the VHF system (see Table 1 for beam widths of the two systems). The characteristics of the meteor echoes detected by the UHF system are similar to those reported by *Zhou and Kelley* [1997]. In the present paper, we emphasize the characteristics of the meteors detected by the VHF system and compare them with those detected by the UHF system. In Figure 6, we plot the hourly rate, altitude of detection, and SNR for the following four group of meteors: (1) those detected by the UHF system (430all or UHF meteors); (2) those detected by the VHF system (47all or VHF meteors); (3) UHF meteors

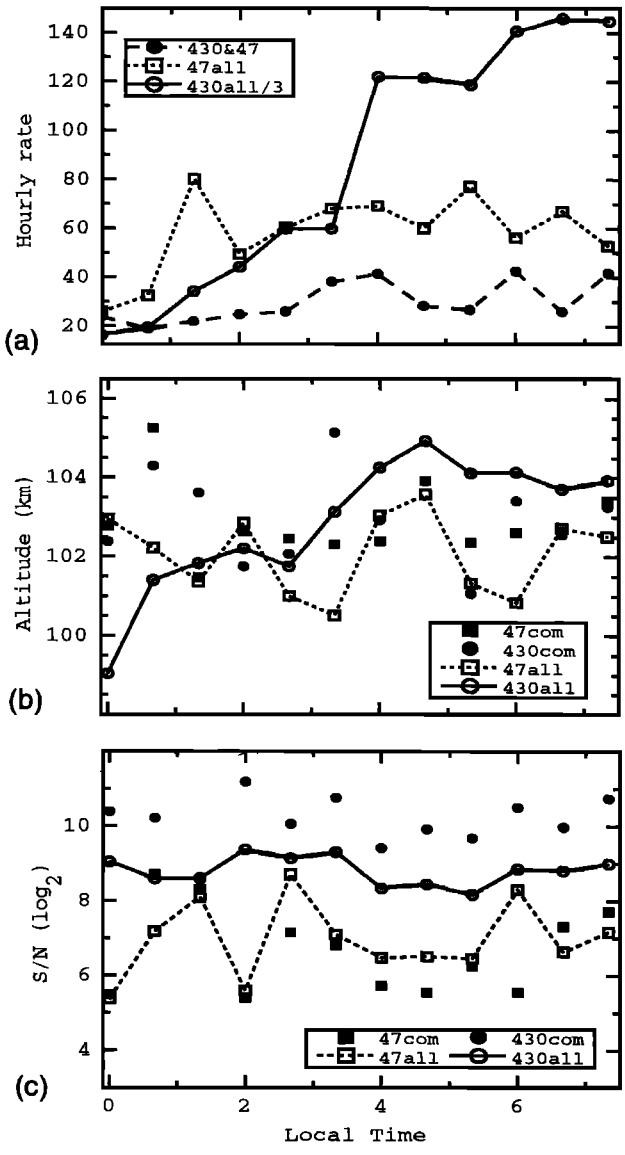

Figure 6. (a) Hourly rate, (b) average altitude, and (c) average signal-to-noise ratio (SNR) as a function of local time for the four groups of meteors defined in the text.

that were also present in the VHF system (430com or UHF common meteors); and (4) VHF meteors that were also present in the UHF system (47com or VHF common meteors). Although the last two groups of meteors are the same in number and hence are the same in Figure 6a, their altitude and SNR attributes are different, as seen in Figures 6b and 6c. The detection altitude, as plotted in Figure 6b, is the altitude where the maximum SNR is found.

The UHF meteor hourly rate shows a dramatic enhancement in the dawn hours, while such an enhancement is less prominent in the VHF data, as seen from Figure 6a. The ratio of dawn to midnight hourly rates may be indicative of the aspect sensitivity for radars having a very narrow beam and pointing near vertically, which apply to our observation. If a system is more sensitive to meteors having a trajectory perpendicular to the radar beam, the midnight and the midday rates are expected to be enhanced. On the other hand, if a system is more sensitive to head-on meteors, the dawn hourly rate is expected to be enhanced. This is because the heliocentric motion of the Earth tends to make the meteor atmospheric entry angle deep (i.e., close to the vertical direction) at dawn and shallow at midnight or noon. The fact that the dawn-to-midnight ratio of the VHF echo rate is much smaller than that of the UHF indicates that the angle of arrival, i.e., the angle between the meteor trajectory and the radar beam direction, of the UHF meteors is likely smaller than that of the VHF meteors on the average. Results from past meteor studies suggest that the dawn-to-midnight ratio is about 1.5 to 2 [*McKinley*, 1961, p. 113]. If we accept that this ratio is free from or corrected for aspect sensitivity, our VHF system is probably not very aspect sensitive. The much larger UHF dawn-to-midnight ratio is consistent with our previous conclusion that the UHF system is likely to be more sensitive to head-on meteors [*Zhou and Kelley*, 1997].

It should be noted that our data-taking and meteor selection scheme may miss some of the cross-beam meteors for both the UHF and VHF systems. Since the percentage of cross-beam meteors (relative to the total number of meteors) is likely higher at midnight than at dawn hours, the dawn-to-midnight ratio of both the UHF and VHF systems can be affected by the beam width and the meteor detection criterion. However, as discussed in section 2, we do not expect the ratio to be changed to the extent of affecting the nature of the above argument.

The temporal variation of the average detection altitude for all the UHF meteors shown in Figure 6b is similar to our previous observations [*Zhou et al.*, 1995; *Zhou and Kelley*, 1997]. The higher altitude around the dawn hours is believed to be due to the higher atmospheric entry velocity at these hours. In contrast to the altitude variation of the UHF meteors, the altitude of the VHF meteors in the dawn hours is not higher than that around midnight. Neglecting the small-scale temporal variations, which are most likely due to the statistical fluctuations because of the small samples available, the altitudes of the VHF meteors remain around 102 km throughout the observation period from 0000 to 0700 LT. The standard deviation of the detection altitude for the common meteors is 5 km, which is comparable with that for all the 430-MHz meteors and 2 km smaller than that for all the VHF meteors.

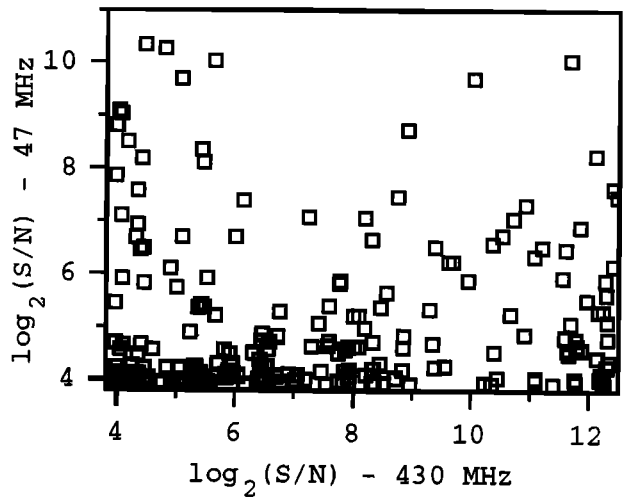

Figure 7. SNR of the VHF radar versus SNR of the UHF radar for the meteors observed by both radars.

On the average, the UHF SNR is about 10 times higher than the VHF SNR for the common meteors, although some of the VHF echoes have an even stronger power return than the corresponding UHF echoes. The standard deviation of SNR is about twice the average of the SNR for each category of meteors. It is of interest to note, from Figure 6c, that while the UHF common meteors have a much larger power than the average UHF meteor, this is not the case for the VHF echoes. One obvious reason is that since the UHF system is more sensitive than the VHF system, the common meteors have to be large enough to be visible to the VHF radar. When the common meteors are compared with other VHF meteors, the former are closer to the beam center and are likely larger than the latter when the antenna gain variation is taken into consideration. For those common meteors, the UHF and the VHF powers are not correlated, in general, as shown in Figure 7. Although antenna pattern difference certainly contributes to the lack of correlation, it is also possible that the scattering mechanisms for the two radars may not be the same.

4. Discussion

4.1. On the Cross Sections of VHF and UHF Head Echoes

We have previously estimated the effective scattering cross section of our UHF observations to be of the order of 10^{-8} m^2 both by calibrating with the ionospheric measurements [*Zhou and Kelley*, 1997] and by using the radar range equation [*Mathews et al.*, 1997]. In the following, we first use the radar range equation to estimate the cross section of meteors detected from the VHF system and then compare it with that of the UHF system.

The SNR of a monostatic radar can be written as

$$\mathrm{SNR} = \frac{P_t G^2 \lambda^2 T_p N_p \sigma}{(4\pi)^3 R^4 L_t L_{tn} L_{sp} \kappa T_s} \tag{5}$$

[*Belcher et al.*, 1993, p.954], where P_t is the peak transmitter power; G is the antenna gain; T_p is the transmitter pulse duration; N_p is the number of coherently integrated pulses; σ is the target effective scattering cross section; R is the target range; L_t, L_{rn}, and L_{sp} are the transmit losses, system nonohmic losses, and the signal processing losses, respectively; κ is the Boltzmann's constant; and T_s is the system noise temperature. The three loss terms amount to about 3 dB typically, and N_p is one in our case. Using the parameters listed in Table 1, the relation between the Arecibo VHF effective scattering cross section σ_{VHF} (in square meters) and SNR at a range of 100 km becomes

$$\sigma_{VHF} = 7 \times 10^{-5} \mathrm{SNR} \tag{6}$$

Using a SNR of 3 as the detection threshold, the limiting cross section for the Arecibo VHF radar is then $2\text{x}10^{-4}$ m^2. The typical SNR in our observation is about 20, and thus a representative effective cross section is of the order of 10^{-3} m^2. Using the parameters listed in Table 1, we further have

$$\frac{\sigma_{VHF}}{\sigma_{UHF}} \approx 10^6 \frac{\mathrm{SNR}_{VHF}}{\mathrm{SNR}_{UHF}} \tag{7}$$

where subscripts VHF and UHF are for the Arecibo VHF and UHF systems, respectively. On the basis of the values in Figure 7, the range of $\sigma_{VHF}/\sigma_{UHF}$ is

$$\frac{\sigma_{VHF}}{\sigma_{UHF}} \approx 3 \times 10^3 \text{ to } 2.5 \times 10^7 \tag{8}$$

On the average, the ratio of UHF SNR to VHF SNR for the common meteors is about 10, which leads to a value of 10^5 for $\sigma_{VHF}/\sigma_{UHF}$ at the beam center.

One main reason for the large spread in $\sigma_{VHF}/\sigma_{UHF}$ is the antenna gain variation at different directions. Since the common meteors are more likely detected in the main lobe of the VHF beam than in the main lobe of the UHF beam, the observed UHF SNR tends to be obtained at a lower gain than assumed. To estimate the possible effect of UHF gain variation, we assume (1) the majority of VHF meteors are more or less evenly distributed in its main lobe; (2) the common meteors are closest to the beam center; and (3) any meteor seen by the VHF radar will also be visible to the UHF radar within a certain radius around the beam center. With these assumptions, the 145 common meteors are roughly distributed within a 0.5° beam radius since the 367 VHF meteors are distributed within about a 1° radius. The UHF antenna has its second sidelobe at 0.5° with the one-way gain reduction (with respect to the beam center) at the far field being ~24 dB [*Mathews et al.*, 1997], which we assume approximately applies to 100 km as well. For a meteor detected 0.5° off the beam center, the two-way UHF antenna gain would be reduced by a factor of $6\text{x}10^4$. If we also assume that low SNR UHF meteors are farther off the beam center, we can apply this reduction factor to the upper value in equation (8), which reduces the spread of $\sigma_{VHF}/\sigma_{UHF}$ significantly. Thus, with the UHF antenna gain variation taken into consideration,

$$\frac{\sigma_{VHF}}{\sigma_{UHF}} \approx 10^3 \tag{9}$$

Since the common UHF echoes are about 20 times stronger than our earlier study [*Zhou and Kelley*, 1997], we estimate the effective scattering cross section of the common UHF meteors to be of the order of 10^{-6} m^2, instead of $3\text{x}10^{-8}$ m^2 for meteors observed within the main lobe. Despite the fact that antenna gain variation is large enough to explain the large spread in $\sigma_{VHF}/\sigma_{UHF}$, we caution the reader that many of the very strong UHF echoes were not accompanied by any VHF echoes. It is possible that meteor atmospheric entry angle, mass, and velocity can also be important in contributing to the large variation in $\sigma_{VHF}/\sigma_{UHF}$.

Given the above caveats, it is of interest to see how the effective scattering cross section for the head echoes depends on the wavelength. Assuming that the effective scattering cross section depends on the wave-

length in the manner of λ^x, equation (8) suggests that x is in the range of 4-8 for the meteors observed by the two radars. If we include the UHF meteors that were not observed by the VHF radar, the lower range of x may potentially extend to negative values. Using the "gain corrected value" of $\sigma_{VHF}/\sigma_{UHF} \simeq 10^3$ for those meteors observed by both radars, we have $x \simeq 3$. In comparison, using the EISCAT 931-MHz and 224-MHz radars, *Wannberg et al.* [1996] reported that $\sigma_{931MHz}/\sigma_{224MHz}$ ranges from 1 to 20 for 18 meteors found in both systems. Since most of the $\sigma_{931MHz}/\sigma_{224MHz}$ ratios cluster around 5, the wavelength dependent factor x can change from 0 to -2, with the most likely value being -1. Whether the difference between the Arecibo and the EISCAT result is due to calibration or scattering process warrants further investigation.

4.2. On the Relative Observability of Trail and Head Echoes

Prior to the experiment, we expected that most of the VHF echoes would be like those shown in Figure 1c. After all, it is the trail echo that makes the meteor wind radar possible. However, during the 7 hours of observation, there were only 10 trail echoes, while nearly 370 VHF head echoes were observed. This indicates that a large antenna aperture can have a drastic effect on echo characteristics.

The smaller number of enduring echoes observed suggests two possibilities: (1) There are very few meteors having shallow atmospheric entry angle, and (2) only very large meteors can produce enduring trail echoes. Since the radar beams were pointed nearly to the vertical direction, most of those meteors observed near the dawn hours had a large radial velocity due to the heliocentric motion of the Earth. If perpendicularity is a necessary condition for observing trail echoes, it would not be surprising that very few of them were observed near the dawn hours. However, around midnight, we expect that the trajectories of some meteors are more or less perpendicular to the radar beam. The number of meteors having a duration longer than 35 ms at each range gate (corresponding to a line-of-sight velocity of 10 km s^{-1}) is indeed far more abundant around midnight than at dawn. This suggests that there were a certain number of meteors which crossed the beam near perpendicularly. Further, as seen from Figure 1b, perpendicularity is not a necessary condition for the observation of trail echoes. The fact that there are only six meteors showing any kind of classical diffusion leads us to believe that only large meteors can produce trail echoes (at least for 47-MHz and above).

Without losing generality, we can assume that any meteor will have a head echo and a trail echo. Let us define the ratio of the head echo power to the trail echo power as γ. To reconcile the difference between our results and those of meteor wind radars, which typically sees far more trail echoes than head echoes, the simplest explanation is to require that γ increase with decreasing meteor size. Such a conclusion is consistent with the observations of *Jones and Webster* [1991], who showed that the probability of visually observed meteors having a head echo increases with radar sensitivity for a detectable scattering cross section larger than 1 m^2. At such a scattering cross section, we hypothesize that γ is smaller than one, which makes some head echoes undetectable. At a scattering cross section of 10^{-3} m^2, γ, in general, is larger than one. If we are not preconditioned to think that a VHF radar should always observe more trail echoes than head echoes, the more logical question to ask from our observation is, Why do some of the trail echoes not have a head echo, instead of vice versa? More specifically, Why do only the three echoes shown in Figures 4d-4f not exhibit any head echo? We can only explain this by believing that these three echoes were due to three large meteors for which the trail echo was stronger than the head echo. Although the head echoes from the three large meteors ought to have a stronger power return than the average head echo, they were not observed most likely because they appeared in the sidelobes.

Our observation has an implication on the design of meteor wind radars. When designing a meteor wind radar, one needs to consider the compromise between the beam width and the sensitivity, given the transmitter power. To increase coverage area, the antenna aperture (or equivalently, the gain) should be as small as possible. On the other hand, one would like to increase the aperture in order to detect smaller meteors also. Since our observation suggests that small meteors may not produce trail echoes, there is an optimal aperture to maximize trail echoes. Although we do not know the exact value of the optimal aperture, it is certain that a 250-m-diameter aperture is too large to be beneficial as a meteor wind radar. (Readers are referred to *Hocking and Thayaparan* [1997], *Valentic et al.* [1997], *Tsutsumi et al.* [1994], and references included therein for wind as well as temperature fluctuation measurements.)

It is of interest to compare our observation with the Jicamarca VHF observation reported by *Chapin and Kudeki* [1994a, b]. The Jicamarca radar operates at a frequency similar to our VHF radar. During their observation, *Chapin and Kudeki* [1994a] transmitted through a 150x150 m^2 dipole field and received with four 37.5x37.5 m^2 arrays for interferometric imagings, while we transmitted and received using an effectively 250-m-in-diameter dish. Since the Jicamarca transmitter is about 80 times more powerful, the two observations have about the same sensitivity. If the scattering mechanisms for the two observations were the same, we would expect relatively few enduring trails in their observation. In addition, their echo rate appears to be much higher than ours. Thus the comparison supports *Chapin and Kudeki*'s [1994b] conclusion that there is an additional scattering mechanism to the classical underdense and overdense scattering for their echoes. As these authors suggested, equatorial plasma instability is likely the cause for the long durations that they observed [*Chapin and Kudeki*, 1994b].

5. Summary and Conclusion

On the night of September 29-30, 1994, we conducted a simultaneous 46.8-MHz and 430-MHz observation of meteor echoes using the Arecibo Observatory 305-m-in-diameter dish. There were a total of 1868 and 367 meteors observed by the UHF and VHF systems, respectively, and 145 meteors were observed by both systems. While the UHF echoes were primarily head echoes, the majority of the VHF echoes were unexpectedly also head echoes. For the 7-hour observation, there were only 10 trail echoes observed. The paucity of trail echoes observed can be explained if the ratio of head echo power to the trail echo power increases with decreasing meteor size. Of the 145 meteors observed by both systems, the VHF power was not correlated with the UHF power. Comparison of VHF and UHF echo rate variation as a function of time suggests that the VHF head echoes are likely not very aspect sensitive. The lack of correlation in power return and potential difference in aspect sensitivity may indicate that the scattering mechanisms responsible for the echoes observed by the two radars are different.

The 10 trail echoes exhibited diverse characteristics and are classified into two large groups based on their range-time behavior. Seven trail echoes were observed to be confined in a narrow altitude range (~2 range gates), which we designated as type 1 echoes. The three other trail echoes, designated as type 2 echoes, showed a clear head echo followed by a trail echo extending over more than three range gates. Of the seven type 1 echoes, six of them showed smooth decaying before they became undetectable. The measured decaying constants were mostly comparable with theoretical underdense *e*-folding constants. Although underdense diffusion appears to be the most visible characteristic of the type 1 echoes, overdense scattering and head echo scattering may also be important at the beginning part of three of the seven type 1 echoes. The echo power in the trail part of type 2 echoes showed large fluctuations, and the trail can simultaneously extend over a 3-km altitude range. These characteristics lead us to suggest that fragmentations may likely occur in type 2 echoes.

Acknowledgments. The Arecibo Observatory is part of the National Astronomy and Ionosphere Center, which is operated by Cornell University under a cooperative agreement with the National Science Foundation. We thank Mike Kelley of Cornell University for his very useful and beneficial comments and discussions. We also thank the observatory staff for their help with the observation and Bill Sisk in particular for his help with the VHF system.

References

Baggaley, W. J., and G. W. Fisher, Measurements of the initial radii of the ionization columns of bright meteors, *Planet. Space Sci., 28*, 575-580, 1980.

Belcher, M. L., J. T. Nessmith, and J. C. Wiltse, Radar, in *The Electrical Engineering Handbook*, edited by R. C. Dorf, pp. 949-974, CRC Press, Boca Raton, Fla., 1993.

Chapin, E., and E. Kudeki, Radar interferometric imaging studies of long-duration meteor echoes observed at Jicamarca, *J. Geophys. Res., 99*, 8937-8949, 1994a.

Chapin, E., and E. Kudeki, Plasma wave excitation on meteor trails in the equatorial electrojet, *Geophys. Res. Lett., 21*, 2433-2436, 1994b.

Djuth, F. T., and J. H. Elder, The VHF meteor radar system used during the Arecibo Initiative in Dynamics of the Atmosphere (AIDA) campaign '89, *J. Atmos. Sol. Terr. Phys., 55*, 229-239, 1993.

Greenhow, J. S., and E. L. Neufeld, The diffusion of ionized meteor trails in the upper atmosphere, *J. Atmos. Sol. Terr. Phys., 6*, 133-140, 1955.

Hocking, W. K., and T. Thayaparan, Simultaneous and colocated observation of winds and tides by MF and meteor radars over London, Canada (43°N, 81°W), during 1994-1996, *Radio Sci., 32*, 833-865, 1997.

Jones, J., and A.R. Webster, Visual and radar studies of meteor head echoes, *Planet. Space Sci., 39*, 873-878, 1991.

Kelley, M. C., C. Alcala, and J. Y. N. Cho, Detection of a meteor contrail and meteoric dust in the Earth's upper mesosphere, *J. Atmos. Sol. Terr. Phys., 60*, 359-369, 1998.

Mathews, J. D., D. D. Meisel, K. P. Hunter, V. S. Getman, and Q. Zhou, Very high resolution studies of micrometeors using the Arecibo 430 MHz radar, *Icarus, 126*, 157-169, 1997.

McKinley, D. W. R., *Meteor Science and Engineering*, McGraw-Hill, New York, 1961.

Meisel, D. D., V. S. Getman, J. D. Mathews, S. C. Jacob, and R. G. Roper, Bolide AIDA: Death of an aubrite meteoroid, *Icarus, 116*, 227-254, 1995.

Nakamura, T., T. Tusda, M. Tsutsumi, K. Kita, T. Uehara, S. Kato, and S. Fukao, Meteor wind observations with the MU radar, *Radio Sci., 26*, 857-869, 1991.

Pellinen-Wannberg, A., and G. Wannberg, Meteor observations with the European incoherent scatter UHF radar, *J. Geophys. Res., 99*, 11,379-11,390, 1994.

Steel, D. I., and W. G. Elford, The height distribution of radio meteors: Comparison of observations at different frequencies on the basis of standard echo theory, *J. Atmos. Sol. Terr. Phys., 53*, 409-417, 1991.

Tsutsumi, M., T. Tsuda, T. Nakamura, and S. Fukao, Temperature fluctuations near the mesopause inferred from meteor observations with the middle and upper atmosphere radar, *Radio Sci., 29*, 599-610, 1994.

Valentic, T. A., J. P. Avery, S. K. Avery, and R. A. Vincent, A comparison of winds measured by meteor radar systems and an MF radar at Buckland Park, *Radio Sci., 32*, 867-874, 1997.

Wannberg, G., A. Pellinen-Wannberg, and A. Westman, An ambiguity-function-based method for analysis of Doppler decompressed radar signals applied to EISCAT measurements of oblique UHF-VHF meteor echoes, *Radio Sci., 31*, 497-518, 1996.

Zhou, Q., and M. C. Kelley, Meteor observation by the Arecibo 430 MHz ISR, II, Results from time-resolved observations, *J. Atmos. Sol. Terr. Phys., 59*, 739-752,1997.

Zhou, Q., C. A. Tepley, and M. P. Sulzer, Meteor observation by the Arecibo 430 MHz ISR, I, Results from time-integrated observations, *J. Atmos. Sol. Terr. Phys., 57*, 421-431, 1995.

J. Y. N. Cho, Department of Earth, Atmospheric, and Planetary Sciences, Massachusetts Institute of Technology, Cambridge, MA 02139. (jcho@pemtropics.mit.edu)

J. D. Mathews, Communications and Space Sciences Laboratory, Pennsylvania State University, State College, PA 16802. (jdm9@psu.edu)

P. Perillat and Q. H. ZHou, Arecibo Observatory, National Astronomy and Ionosphere Center, Arecibo, PR 00612. (phil@naic.edu; zhou@naic.edu)

(Received November 17, 1997; revised July 13, 1998; accepted July 21, 1998.)